Hindawi
Geofluids
Volume 2020, Article ID 2592693, 17 pages
https://doi.org/10.1155/2020/2592693

Research Article

A Parametric Study of Coupled Hydromechanical Behaviors Induced by Shallow Water Flow in Shallow Sediments in Deepwater Drilling Based on Numerical Modeling

Xuyang Guo,[1,2,3] **Yan Jin**,[1,2] **and Botao Lin**[1,2]

[1]*State Key Laboratory of Petroleum Resources and Prospecting, China University of Petroleum (Beijing), 18 Fuxue Rd, Beijing 102249, China*
[2]*College of Petroleum Engineering, China University of Petroleum (Beijing), 18 Fuxue Rd, Beijing 102249, China*
[3]*Department of Petroleum Engineering, China University of Petroleum (Beijing) at Karamay, 355 Anding Rd, Karamay, Xinjiang 834000, China*

Correspondence should be addressed to Xuyang Guo; xguo@cup.edu.cn

Received 18 September 2019; Accepted 7 May 2020; Published 4 August 2020

Academic Editor: Ye Zhang

Copyright © 2020 Xuyang Guo et al. This is an open access article distributed under the Creative Commons Attribution License, which permits unrestricted use, distribution, and reproduction in any medium, provided the original work is properly cited.

Shallow water flow is a geohazard encountered in deepwater drilling. It is often characterized by excessive water flow into the wellbore caused by the pressure difference between overpressured sediments and the wellbore, and it usually leads to serious well control problems and may eventually result in the loss of a well. Many research efforts focused on the identification of shallow water flow zones and the associated water flow in the drilled wellbore. Not many studies investigated the coupled hydromechanical behaviors in sediments during the occurrence of shallow water flow, while such behaviors are directly related to uncontrolled flow in the wellbore and solid deformation. Based on a coupled hydraulic-mechanical model and finite element methods, this work investigates the temporal-spatial evolutions of near-well pressure and stress induced by shallow water flow. Hydraulic behaviors in the deepwater shallow sediments are described by saturated fluid flow in porous media while mechanical behaviors in the sediments are depicted by linear elasticity. Finite element methods are used for the numerical solution to the coupled hydraulic-mechanical formulation. The study then conducts a series of parametric studies to quantitatively understand the effects of relevant parameters on pressure, stress, and uncontrolled flow into the wellbore. Results indicate that overpressure has the most significant impact while Young's modulus has the most limited impact on spatial-temporal pressure/stress evolutions and the uncontrolled water production in the wellbore. Permeability, porosity, water viscosity, and water compressibility all have certain effects on near-well physical characteristics and wellbore water production. In addition, it is noted that pressure drainage and induced stress are more significant when it is closer to the wellbore. This numerical study helps to quantitatively identify the most influential parameters related to shallow water flow and calculates the water mass flow loaded in the wellbore.

1. Introduction

Shallow water flow is a type of geohazard encountered in deepwater drilling operations where water flows toward the well are induced as a result of drilling through overpressured deepwater shallow sediments. Occurrences of shallow water flow in deepwater drilling sites have been reported since 1984 worldwide from the Gulf of Mexico, West of the Shetlands, the Norwegian Sea, the North Sea, South China Sea, offshore Malaysia, etc. [1–6]. Shallow water flows lead to major or minor flows and sand production in drilled wells and cause well control problems, and in extreme cases, they result in the loss of deepwater wells [2]. They largely reduce the hydrocarbon extraction efficiency and increase costs in deepwater sites.

The pressure gradient between the wellbore and the overpressured sediments buried deep below the mud line is the driving force that induces shallow water flows during

deepwater drilling [1, 7]. Therefore, it is important to identify zones prone to shallow water flows before the deepwater drilling operation. Specifically, seismic data are widely used for the identification and characterization of shallow water flow zones, and successful quantitative understanding of deepwater shallow sediments was reported from deepwater assets worldwide [3–6, 8–13], where deepwater well locations were optimized and the risk of shallow water flow was reduced.

Although the interpretation of seismic data is effective in reducing the risk of drilling in shallow water flow zones in some cases, shallow water flows still occur in certain deepwater sites [14–18]. Thus, when shallow water flows are induced, it is especially important to characterize the flows in the overpressured sedimentary layers and in the wellbore. Some studies were carried out to model and quantify the properties associated with shallow water flow layers, the characteristics of shallow water flows, and their impact on the sedimentary layers and the wellbore. Based on data from geotechnical wells, Ostermeier et al. [19] established the correlations between overpressures, porosity, depth, and clay content for the deepwater Gulf of Mexico. This study quantified the regional trends of relevant properties which helped to facilitate deepwater operations in the Gulf of Mexico. Huffman and Castagna [20] also quantitatively investigated the petrophysical properties in the Gulf of Mexico and indicated that the effective stress caused by water flows in sediment layers can be an important factor that contributes to the failure of shallow water flow zones. Binh et al. [21] formulated the porosity-permeability correlations in Ursa Basin and applied a fully coupled simulator to simulate the fluid flows in shallow overpressure zones. In the same region, Reece et al. [22] correlated compressibility, permeability, and porosity which are key parameters governing the fluid flow in the formation. Gong et al. [23] and Ren et al. [24] proposed a numerical model that simulates water and sand flows induced by deepwater drilling through overpressured zones, where the heavy oil flow is used as a proxy which represents the sand flow. In their shallow water flow model, both water and sand flows strictly follow Darcy's law and petroleum reservoir simulation practices were widely implemented. Based on the commercial simulator FLAC3D which couples fluid flow and geomechanics, Sun et al. [25] simulated the fluid flow behaviors which obey Darcy's law and the rock deformation which is based on Cam-Clay material assumptions. Zhang et al. [5] introduced a prediction model, which includes a hybrid computational approach. This approach correlates pressure, velocity, and seismic data with accuracy substantiated by experimental data.

According to the literature review, numerical modeling is effective in the characterization of shallow water flows. Specifically, Darcy's law, the equation describing subsurface flow in porous media, was proved to be useful and has been successfully used in the quantification of shallow water flows in the porous media buried beneath the mud line [5, 23–25]. Meanwhile, it is noted that not many studies were carried out to investigate the coupled behaviors of subsurface fluid flow and rock deformation in the context of deepwater-drilling-induced shallow water flows. Besides, a comprehensive sensitivity analysis, which quantifies the effects of relevant fluid and rock properties on shallow water flow sedimentary layers can serve as a reference for deepwater drilling through layers with this type of geohazard risk.

In this work, the temporal and spatial evolutions of pore pressure and rock deformation associated with shallow water flows caused by deepwater drilling through porous media of shallow sediments beneath the mud line are quantified. A finite element model which couples subsurface porous media flow and rock deformation is introduced. A set of sensitivity analyses is then carried out in a parametric study of the relevant fluid and rock properties and their impact on the shallow water flow. Based on the numerical results, areas prone to significant rock deformation in the porous media are identified. The mass flow of water from the porous media into the wellbore is also calculated, which provides a reference for geohazard remediation. The contribution of this work lies in its use of a numerical model that couples shallow water flows and rock deformation in a comprehensive and quantitative parametric study of the near-well coupled hydromechanical behaviors in shallow sediments.

2. Numerical Model

The sediments buried in shallow water flow zones can be treated as fully saturated porous media [5, 20, 23, 24]. In a coupled hydraulic-mechanical problem, both subsurface water flow and rock deformation should be considered. Terzaghi [26, 27] and Biot [28, 29] consolidation theories are the foundation for the poroelastic behaviors in hydraulic-mechanical interactions. Based on these theories, many numerical models have been developed to describe the coupled processes for deformation in fully saturated porous media [30–33].

A numerical model that describes the single-phase water flow in porous media and the deformation of the porous media is derived in this section. The model can be used to simulate the shallow water flow in the sediments.

2.1. Formulation of the Water Flow in Sediments. The subsurface water flow problem is based on mass conservation, and it can be formulated as

$$\frac{\partial(\phi\rho_w)}{\partial t} + \nabla\bullet[\phi\rho_w(\boldsymbol{v_{ws}} + \boldsymbol{v_s})] = \dot{m}_w, \tag{1}$$

where ϕ is the porosity of the porous media; ρ_w is the density of water; t is time; $\dot{m}_w$ is the mass flow rate, where $\dot{m}_w = \rho_w q_w$. q_w is the volumetric flow rate. The fully saturated porous media are treated as two phases: the water phase and the solid phase. $\boldsymbol{v_{ws}}$ is the relative velocity between the solid phase and the water phase, and $\boldsymbol{v_s}$ is the velocity of the solid phase (deformation rate). Therefore, the term $\boldsymbol{v_{ws}} + \boldsymbol{v_s}$ represents the interstitial water velocity which describes the velocity of water molecules [34, 35]. In mass conservation concepts, $\partial(\phi\rho_w)/\partial t$ is the accumulation term; $\nabla\bullet[\phi\rho_w(\boldsymbol{v_{ws}} + \boldsymbol{v_s})]$ is the flux term; $\dot{m}_w$ is the sink/source term.

Eq. (1) can be expanded to

$$\frac{\partial(\phi\rho_w)}{\partial t}+\nabla\bullet(\phi\rho_w\boldsymbol{v_{ws}})+\nabla\bullet(\phi\rho_w\boldsymbol{v_s})=\rho_w q_w. \quad (2)$$

The flux term can be further expanded by Darcy's law as

$$\boldsymbol{v_w}=\phi\boldsymbol{v_{ws}}=-\frac{\boldsymbol{k}}{\mu_w}\nabla p, \quad (3)$$

where $\boldsymbol{k}$ is a second-order permeability tensor that represents the ability of water to flow in the sediments; μ_w is the water viscosity; p is the water phase pressure. The effect of gravity is neglected.

Combining Darcy's law (Eq. (3)) with the mass balance equation (Eq. (2)),

$$\frac{\partial(\phi\rho_w)}{\partial t}+\nabla\bullet(\rho_w\boldsymbol{v_w})+\boldsymbol{v_s}\bullet\nabla(\phi\rho_w)+\phi\rho_w\nabla\bullet\boldsymbol{v_s}=\rho_w q_w. \quad (4)$$

Considering material derivatives in continuum mechanics,

$$\frac{d(\phi\rho_w)}{dt}=\frac{\partial(\phi\rho_w)}{\partial t}+\boldsymbol{v_s}\bullet\nabla(\phi\rho_w). \quad (5)$$

Taking into account the assumption of infinitesimal deformation $\partial(\phi\rho_w)/\partial t \gg \boldsymbol{v_s}\bullet\nabla(\phi\rho_w)$, Eq. (5) can be rewritten as

$$\frac{d(\phi\rho_w)}{dt}\approx\frac{\partial(\phi\rho_w)}{\partial t}. \quad (6)$$

Incorporating Eq. (6) into Eq. (4),

$$\frac{\partial(\phi\rho_w)}{\partial t}+\nabla\bullet(\rho_w\boldsymbol{v_w})+\phi\rho_w\nabla\bullet\boldsymbol{v_s}=\rho_w q_w. \quad (7)$$

Water is a compressible fluid. Its compressibility c_w is related to pressure and fluid density by definition as

$$c_w=\frac{1}{\rho_w}\frac{\partial\rho_w}{\partial p}. \quad (8)$$

Thus, Eq. (7) can be expressed as

$$\rho_w\frac{\partial\phi}{\partial t}+\phi\rho_w c_w\frac{\partial p}{\partial t}+\nabla\bullet(\rho_w\boldsymbol{v_w})+\phi\rho_w\nabla\bullet\boldsymbol{v_s}=\rho_w q_w. \quad (9)$$

Eq. (9) is the governing equation of the subsurface water flow in the porous media in the sediments.

2.2. Formulation of Deformation of Sediments. The deformation of the sediments can be further described by the momentum balance based on the quasi-static assumption [36],

$$\nabla\bullet\boldsymbol{\sigma}=0, \quad (10)$$

where $\boldsymbol{\sigma}$ is the Cauchy stress tensor.

The Cauchy stress tensor can be written as

$$\boldsymbol{\sigma}=\boldsymbol{\sigma}_0-b(p-p_0)\boldsymbol{I}+C_{dr}:\varepsilon, \quad (11)$$

where the subscript 0 denotes the initial condition; $\boldsymbol{I}$ is the identity tensor; C_{dr} is the fourth-order stiffness tensor; ε is the strain tensor which can be expressed as $\varepsilon=\nabla^s\boldsymbol{u}=1/2(\nabla^T\boldsymbol{u}+\nabla\boldsymbol{u})$, and ∇^s is the symmetric gradient operator.

A linear relationship between stress and strain is considered in the deformation problem. While this assumption introduces limitations when dealing with very weak sediments, it is included in the model based on relevant experimental and modeling studies in the literature. On the one hand, based on experimental tests on mechanical properties of samples from the South China Sea and the Gulf of Mexico, the stress-strain relation can exhibit behaviors of brittle clays. In some cases, linear elastic behaviors were captured as well [37, 38]. One the other hand, since this study is more emphasized on the flow-induced stress evolution, the linear elasticity assumption is taken as a treatment used for building coupled hydromechanical models [39, 40].

2.3. Coupling Water Flow and Deformation. In Eq. (9), based on the poroelasticity assumption, porosity ϕ is a function of time. According to Geertsma [41] and Biot and Willis [42], the time derivative of porosity is expressed as

$$\frac{\partial\phi}{\partial t}=\frac{b-\phi}{K_s}\frac{\partial p}{\partial t}+(b-\phi)\frac{\partial\varepsilon_v}{\partial t}, \quad (12)$$

where b is the Biot's coefficient and ε_v is the volumetric strain.

The stress sensitivity of permeability is considered via a porosity-permeability relationship as in Eq. (13)

$$k=k_0\exp\left[\gamma\left(\frac{\phi}{\phi_0}\right)-1\right], \quad (13)$$

where γ is a permeability-porosity constant.

By definition, the solid phase rate $\boldsymbol{v_s}$, the displacement $\boldsymbol{u}$, and the volumetric strain can be related as

$$\boldsymbol{v_s}=\frac{\partial\boldsymbol{u}}{\partial t}, \quad (14)$$

$$\varepsilon_v=\nabla\bullet\boldsymbol{u}. \quad (15)$$

Incorporating Eqs. (12), (13), (14) and (15) into Eq. (9),

$$\left(\frac{b-\phi}{K_s}+\phi c_w\right)\frac{\partial p}{\partial t}+b\frac{\partial\varepsilon_v}{\partial t}+\nabla\bullet(\boldsymbol{v_w})=q_w. \quad (16)$$

Eq. (16) is the governing equation that fully couples the water flow with the deformation of the sediments.

2.4. Numerical Solution. The finite difference method is used to achieve the time discretization while finite element methods are used to achieve the space discretization. The

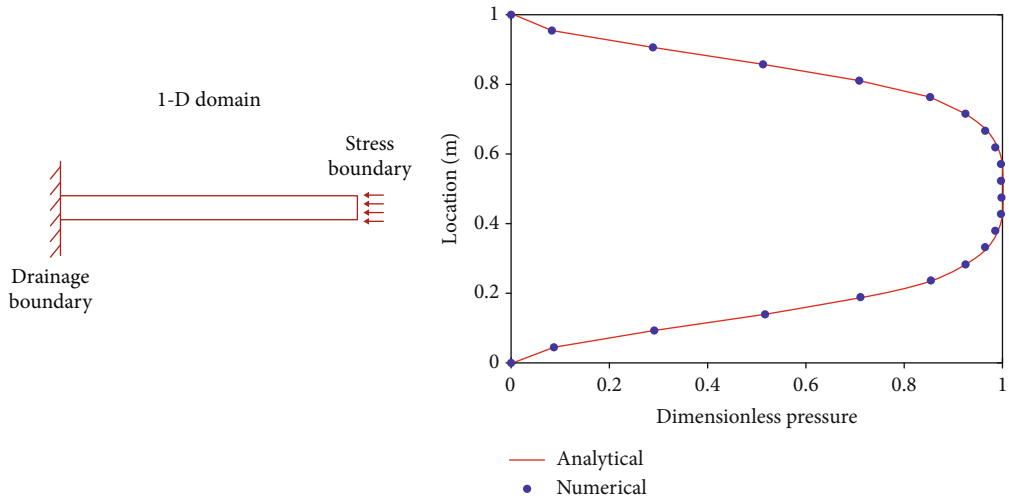

(a) Geometry of the problem (b) Validation result

Figure 1: Validation with Terzaghi's problem.

backward Euler method is used for time stepping as it guarantees the stability of the numerical solution.

In the finite element analysis, primary variables of pressure, fluid velocity, and displacement are solved. The solution of p_h, v_h, u_h for pressure, fluid velocity, and displacement is analyzed in the space of DG × RT × CG which consists of discontinuous Galerkin, Raviart-Thomas, and standard/continuous Galerkin. The corresponding weak forms are as

$$\left(\psi, \left(\frac{b-\varnothing}{K_s}+\varnothing c_w\right)\frac{p^{n+1}-p^n}{\Delta t}\right)_\Omega + \left(\psi, b\frac{\varepsilon_v^{n+1}-\varepsilon_v^n}{\Delta t}\right)_\Omega + \left(\psi, \nabla\bullet v_w^{n+1}\right)_\Omega = (\psi, q_w)_\Omega, \tag{17}$$

$$\left(\omega, \frac{1}{\lambda_w k}v_w^{n+1}\right)_\Omega - \left(\nabla\bullet\omega, p^{n+1}\right)_\Omega = 0, \tag{18}$$

$$(-\varepsilon(\varphi), \sigma_0)_\Omega - 2\left(\varepsilon(\varphi), \mu\varepsilon\left(u^{n+1}\right)\right)_\Omega - \left(\lambda(\nabla\bullet\varphi), \left(\nabla\bullet u^{n+1}\right)\right)_\Omega + \left(\nabla\bullet\varphi, b\left(p^{n+1}-p_0\right)\right)_\Omega = -(\varphi, t)_\Gamma, \tag{19}$$

where ψ, ω, φ are test functions; n is the current time step; p_0 is the initial pressure. The discontinuous basis functions help to incorporate the upstream weighting technique in the scheme of the coupled model and enhance the stability in the numerical solution. The Raviart-Thomas method is intuitively suitable for the velocity equation (Eq. (18)), which describes the flow through the face between two elements. Thus, it ensures accuracy and stability when solving for velocity.

Table 1: Parameters for model validation.

Property name	Value
Domain length	1.00 m
Cell length	0.05 m
Permeability	6.5×10^{-15} m^2
Porosity	43%
Young's modulus	0.6 GPa
Solid density	2600 kg/m^3
Fluid density	728 kg/m^3
Viscosity	8.6×10^{-4} Pa · s
Stress boundary	20 MPa

2.5. Model Validation. Terzaghi's problem [26, 27] captures the pressure buildup caused by external stress, which is widely used in validating numerical coupled hydromechanical models. The detailed analytical solution for this consolidation process can be found in Verruijt [43], which solves for the pressure distribution along the 1-D domain at a certain time step. The exertion of stress on the boundary consolidates the porous media and increases pore pressure while the drainage boundary contributes to the decrease in pressure. At an intermediate time, the center of the pressure profile is higher due to the stress boundary while the profile gets lower near the boundaries due to pressure drainage. The validation model is established with certain input parameters (10.2118/182665-MS) [44]. The validation model is shown in Figure 1(a), and the parameters are recorded in Table 1. The parameters provide information for the model geometry, porous media flow properties, and mechanical properties of the saturated porous media, which are necessary inputs for the analytical and numerical solutions. The matching between the analytical solution and the numerical solution calculated using the model in this study is shown in Figure 2(b). Note that the matching is obtained

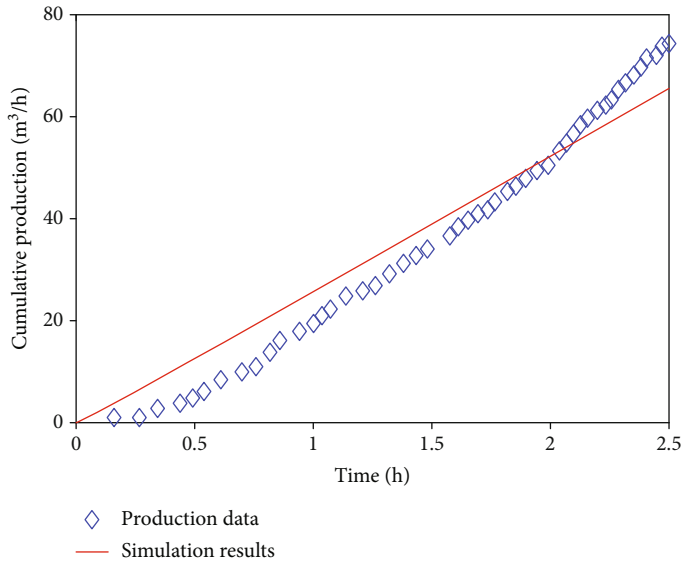

Figure 2: Verification for water production against published production data.

with a dimensionless time t_d of 0.03 and the accuracy of the numerical model is validated. The dimensionless time is defined as

$$t_d = \frac{tc_v}{L_f^2}, \tag{20}$$

$$c_v = \frac{k}{\mu\left((1/K_{dr}) + \phi c_f\right)}, \tag{21}$$

where L_f is the location; K_{dr} is the drained modulus; c_f is the fluid compressibility; c_v is the consolidation coefficient. Figure 1(b) indicates that numerical and analytical solutions match well, and the numerical model can accurately calculate the pressure profile for Terzaghi's problem.

2.6. Verification of Water Production. To further verify the numerical model, water production caused by shallow water flow in a deepwater drilling scenario is simulated and verified against the published data from Gong et al. [23]. The water depth is 1500 m with shallow water flow encountered between 500 to 600 m below the mudline. The overpressure in the shallow water flow zone is represented by a pressure factor of 1.2. Related parameters are in Table 2, which are used for the numerical simulation.

The results are shown in Figure 2. By modifying the well constraint, simulation results generally match with the water production data. The simulated production is higher than the published data before 2 hours, and the trend reverses afterward. The maximum error of 11.8% is obtained at 2.5 hours. It is noted that the cumulative production increases rapidly since the pressure drive is strong for the first 2.5 hours of shallow water flow.

Table 2: Parameters for the water production verification case.

Parameter	Value
Water depth	1500 m
Shallow water flow depth	500-600 m below mudline
Area	3600 m^2 (60 m by 60 m square)
Permeability	3000 mD
Water density	1035 kg/m^3
Density of sediments	2600 kg/m^3
Formation pressure	24.3 MPa
Porosity	40%
Simulation time for the induced shallow water flow	2.5 hours

3. Simulation of Coupled Hydromechanical Behaviors

3.1. Model Geometry. Shallow water flows are induced by the pressure difference between the overpressured sediments and the fluids in the drilled wellbore. This process can be simulated in a shallow water flow model that consists of the porous media of the sediments and the wellbore which penetrates through the porous media as in Figure 3.

Figure 3(a) is the top view showing the 2D horizontal plane with the wellbore at the center of the domain. Figure 3(a) is a 2D horizontal slice taken from Figure 3(b) which shows the 3D conceptual model for the shallow water flow layer: the permeable layer is bounded by two impermeable shale layers that act as seals. The permeable layer is the target domain where 2D coupled hydraulic-mechanical processes are simulated in this study. The wellbore is drilled through the overpressure layers, introducing pressure gradients between the well and the porous media. The pressure gradients result in the water flow from the porous media into the wellbore.

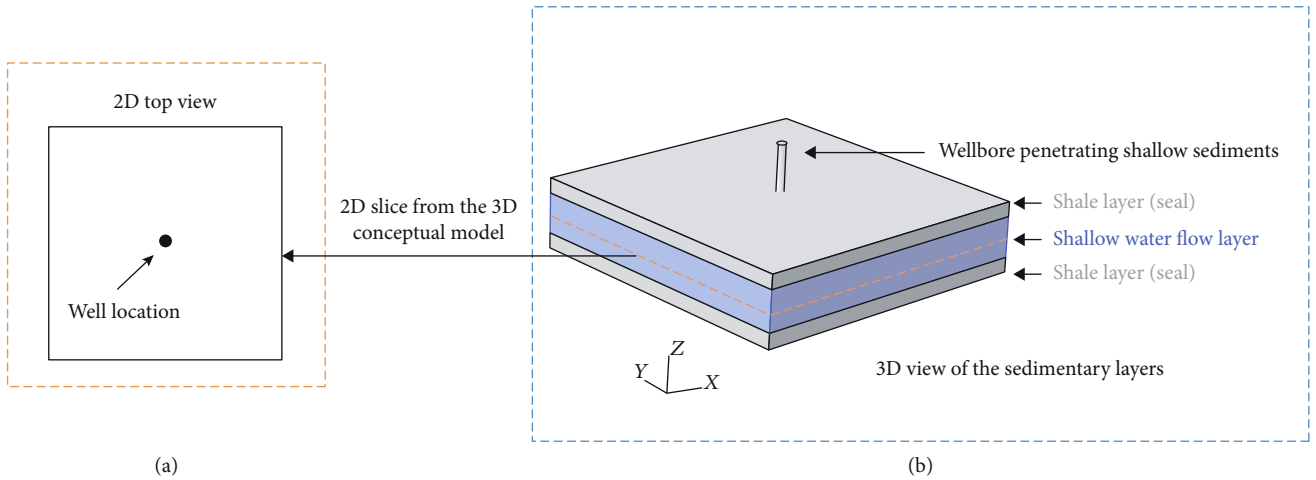

Figure 3: (a) 2D domain of the numerical model in this study and (b) 3D conceptual model of the target area.

3.2. Input Parameters. Published data from the Gulf of Mexico [19, 21, 37] are used for the values of parameters in the 2D model. They provide realistic overpressure data, mechanical properties of sediments, and hydraulic properties in the Gulf of Mexico. The parameters used for the base case of the numerical study are recorded in Table 3.

3.3. Base Case Characteristics. Base case numerical results for 2D pressure and von Mises stress distributions after one day of shallow water flow are shown in Figure 4. The sink in Figure 4(a) and the peak in Figure 4(b) represent the location of the wellbore ($X = 300$ m, $Y = 300$ m). An observation line (X from 300 m to 600 m, $Y = 300$ m) is used to plot 1D characteristic distribution. Figure 5 plots the 1D characteristics of pressure and stress at three time steps from the wellbore to the domain boundary along $Y = 300$ m. The sink in Figure 4(a) is caused by the fact that the hydrostatic pressure in the wellbore is lower than the overpressure in the sediment layer. Figure 5(a) indicates that due to the effect of the sink, the pressure in the porous layer decreases with time. Figure 4(b) shows that the peak of the fluid-flow-induced stress is at the wellbore, and the stress decreases as it moves away from the wellbore. This is explained by the Biot's consolidation theory: areas near the wellbore experience high water flow velocities which induce large pore volume changes; such changes then induce large stress magnitudes. Figure 5(b) shows that, as the pressure difference between the wellbore and the porous layer decreases with time, the stress magnitude decreases. This is because shallow water flow velocity and the pressure difference between the wellbore and the porous layer decrease with time, and the magnitude of the induced stress decreases accordingly. Figures 4(b) and 5(b) indicate that the von Mises stress profile is high within 100 m of the wellbore. Since the von Mises criterion indicates how the region enters plasticity and plasticity tends to induce sand production [45], it is implied that the risk of sand production around the wellbore is higher than the far-field.

Table 3: Parameters for the base case of the numerical study.

Parameter	Value
Mesh size	600 m by 600 m
Coordinates of wellbore location	(300 m, 300 m)
Wellbore radius	0.1 m
Water density	1000 kg/m^3
Water viscosity	0.002 Pa·s
Water compressibility	4.5×10^{-10} 1/Pa
Density of porous media	2350 kg/m^2
Porosity of porous media	0.4
Permeability of porous media	1.0×10^{-12} m^2
Compressibility of porous media	5.0×10^{-10} 1/Pa
Young's modulus of porous media	15 GPa
Poisson's ratio of porous media	0.25
Biot's coefficient	1
Hydrostatic pressure in the wellbore	10.9 MPa
Pore pressure in the overpressured layer	13.6 MPa
Boundary condition for water flow	No flow Neumann boundary
Boundary condition for deformation	Fixed displacement
Simulation time for the induced shallow water flow	1 day

4. Numerical Results and Discussion

Once the model and the parameters for the base case are set up, a set of numerical investigations are carried out to study the effects of relevant fluid and solid parameters on the characteristics of shallow water flow in the sediments. In this section, sensitivity analyses are conducted for the parameters of overpressure, permeability, porosity, water viscosity, Young's modulus, and water compressibility. Numerical results of pore pressure, stress, and water production in the well are presented, as these results are of special interest in the quantitative understanding of shallow water flow from porous media to the wellbore.

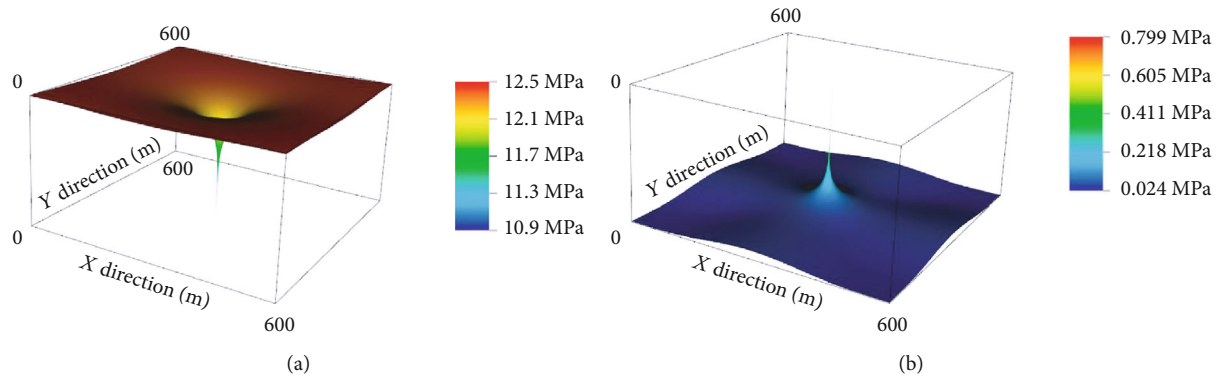

Figure 4: Surface maps of (a) pressure distribution after one day of shallow water flow and (b) von Mises stress distribution after one day of shallow water flow in the sediments.

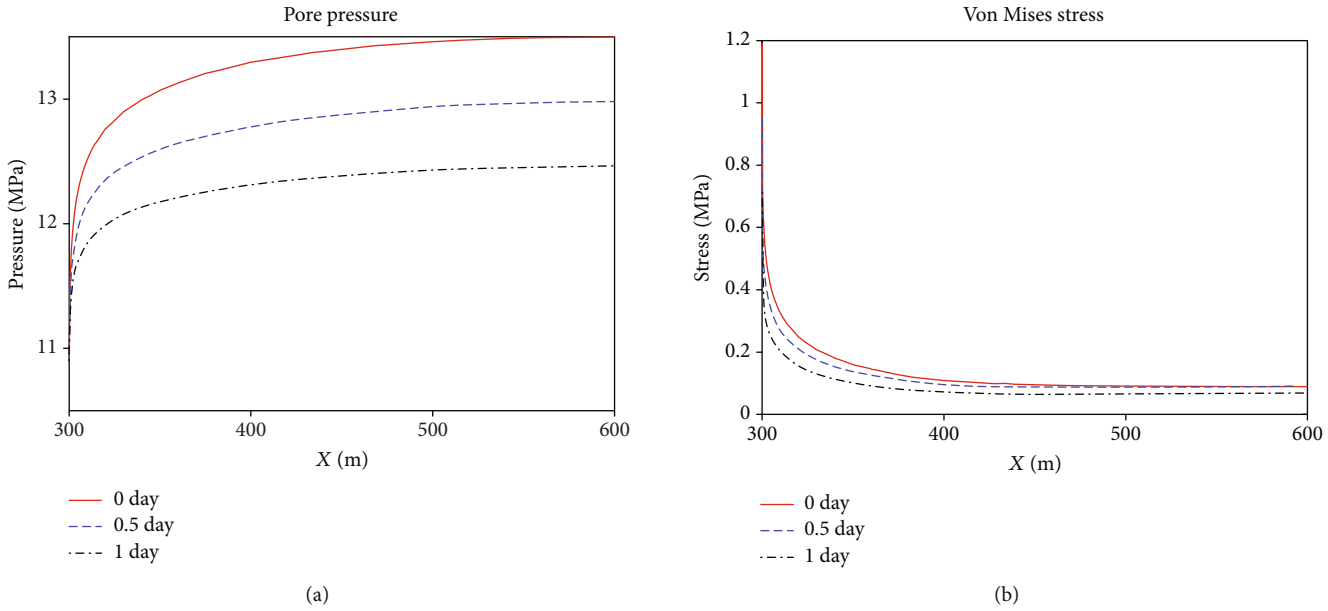

Figure 5: 1D distribution from the wellbore to the boundary of the domain for (a) pressure and (b) von Mises stress; plots for data along $Y = 300$ m.

For space and time characterization of stress evolutions in the sediments, the von Mises stress is calculated. This is because the von Mises stress follows the maximum distortion energy theory and it helps to establish the profile that can be used to identify the area entering plastic behaviors. Therefore, it can denote the area prone to yielding behaviors and sand production.

In this study, water production in the well represents the uncontrolled mass flow of shallow water flow into the wellbore. Quantified and ranked parametric effects are provided in the end.

4.1. Overpressure. Overpressure is the pressure difference between the porous layer and the hydrostatic pressure in the wellbore. The geological environment plays an important role in overpressure and the uncertainty in overpressure measurement is usually high [4]. Wellbore hydrostatic pressure is kept constant and porous layer pressure is varied. Three overpressure values are investigated: 1.35 MPa, 2.70 MPa (base case), and 4.05 MPa. Other parameters are kept the same as the base case.

Figure 6 shows the 1D pressure distribution from the wellbore to the domain boundary along $Y = 300$ m after 0.5 day and 1 day of shallow water flow. Figure 7 presents the 1D stress distribution from the wellbore to the domain boundary along $Y = 300$ m after 0.5 day and 1 day of shallow water flow.

In Figure 6, a greater overpressure leads to a higher pressure distribution profile. This is intuitive as a greater overpressure indicates higher pore pressure in the porous media. The pressure profiles also decrease with time as the porous media fluid is drained and the pore pressure is depleted by the wellbore. In Figure 7, overpressure is negatively correlated with stress magnitude. This is because greater overpressure results in greater drainage of fluid and a greater pressure difference between the wellbore and the

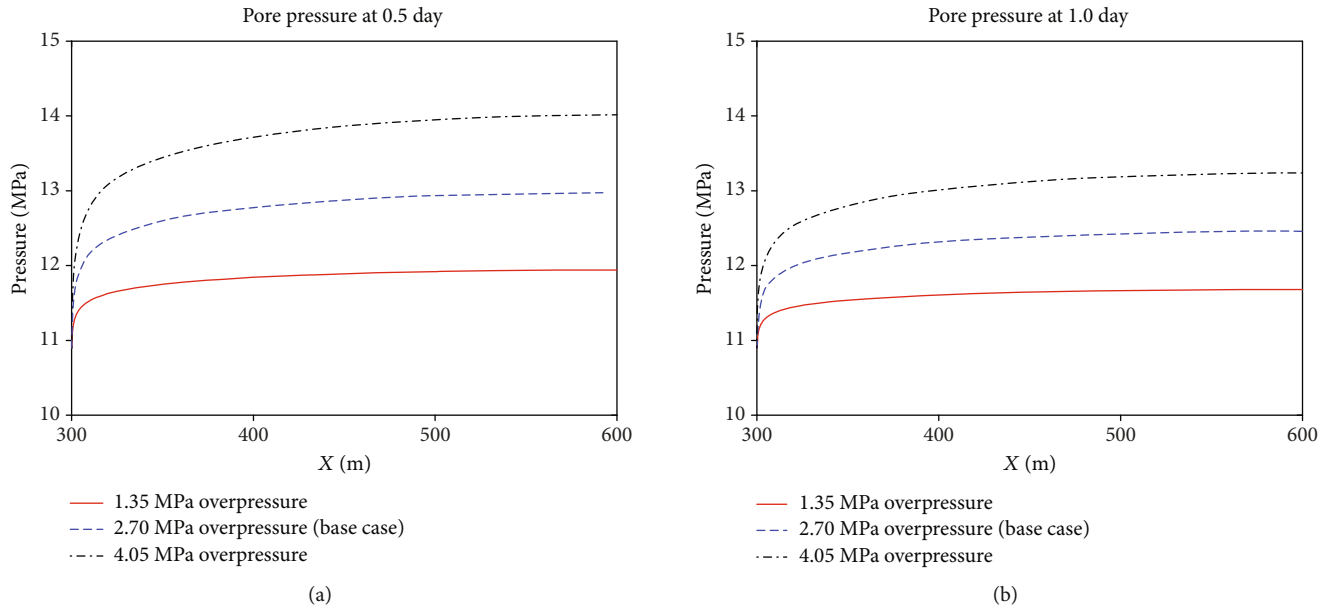

Figure 6: 1D pressure distribution from the wellbore to the domain boundary along $Y = 300$ m after (a) 0.5 day and (b) 1 day of shallow water flow for overpressure sensitivity.

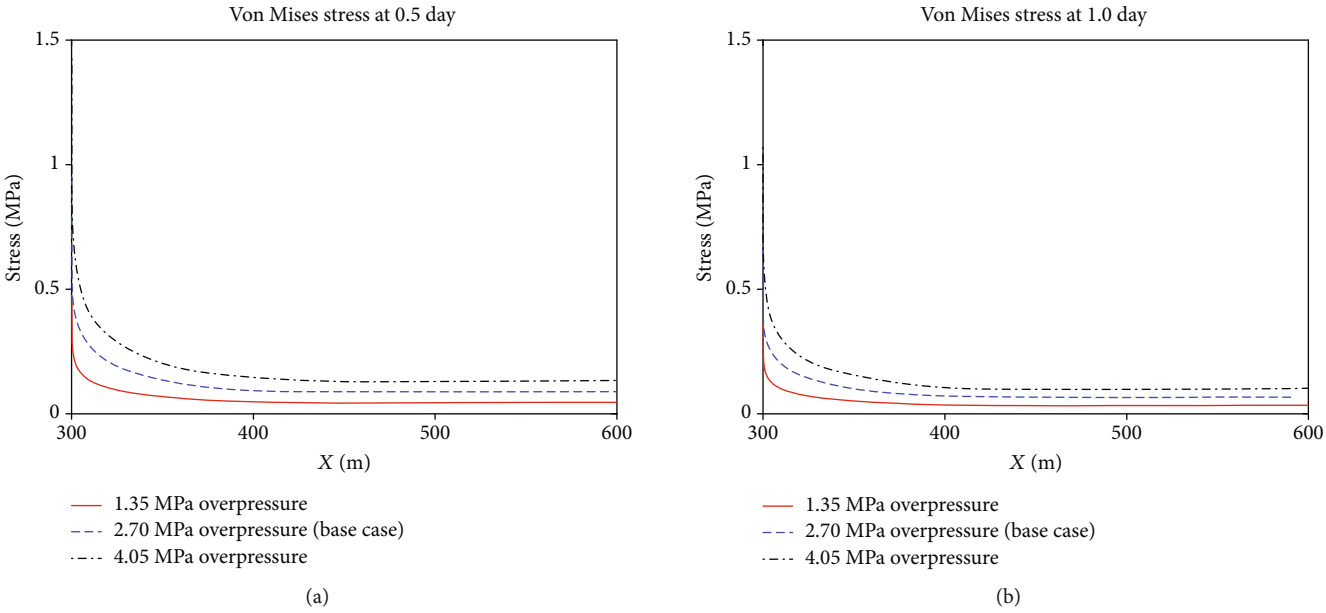

Figure 7: 1D stress distribution from the wellbore to the domain boundary along $Y = 300$ m after (a) 0.5 day and (b) 1 day of shallow water flow for overpressure sensitivity.

porous layer, indicating more pore volume changes and stronger deformation [28, 29]. Besides, stress profiles decrease with time, indicating the decrease in pressure differences between the wellbore and the porous media also has an impact on the decrease of induced stress. Greater von Mises stress indicates the deformation of solids is stronger and the area is more prone to sand production.

Water production in the wellbore is a major negative impact of shallow water flow on deepwater drilling as water production causes well control problems. Figure 8 shows the cumulative water production in the wellbore caused by shallow water flow for three different overpressure scenarios. Since a 2D model is used in the study, water production mass is normalized by the thickness, and the production is reported in kg/m. Overpressure is positively correlated with the cumulative water production, since higher overpressure forms a greater pressure gradient which serves as the driving force for water flow in the wellbore. The total water production of the 4.05 MPa overpressure case is about three times of that in the 1.35 MPa overpressure case. This numerical result quantitatively characterizes the water mass loaded in the wellbore.

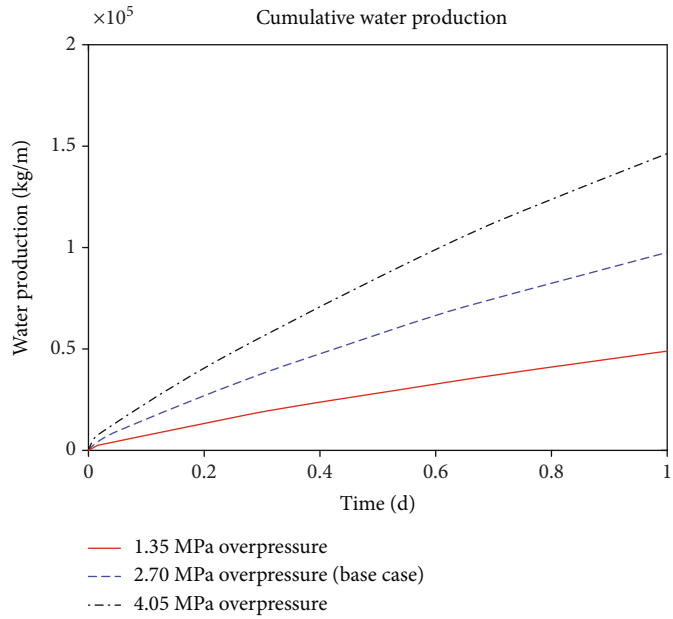

Figure 8: Cumulative water production at the wellbore during one day of shallow water flow for overpressure sensitivity.

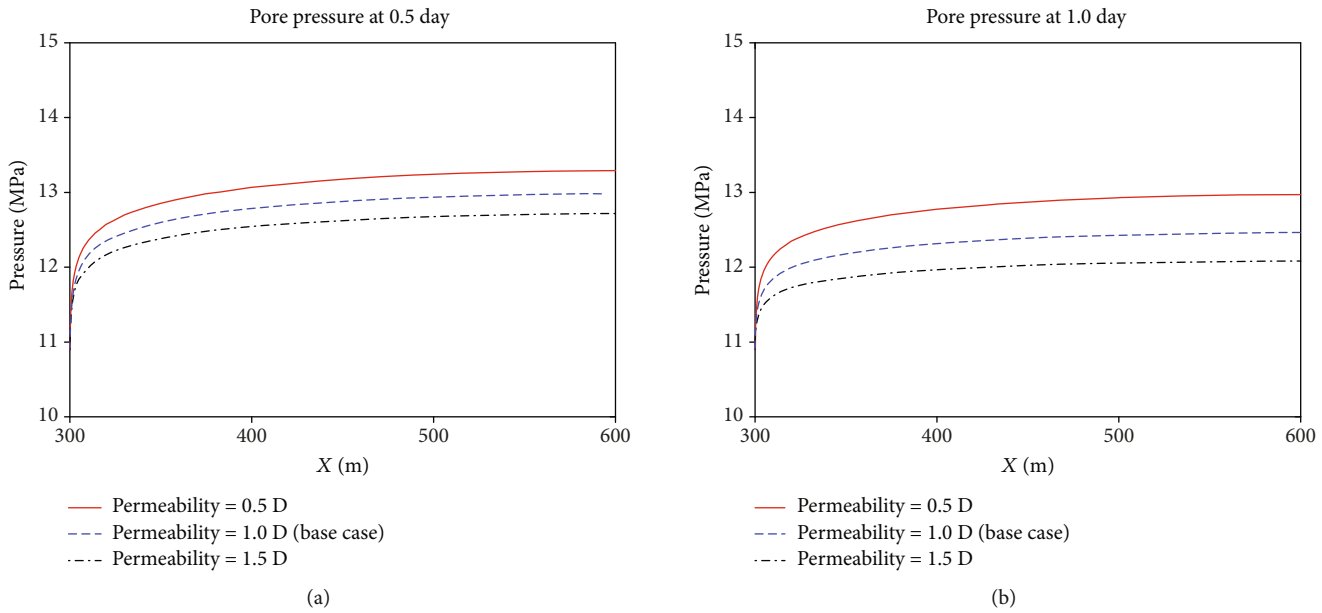

Figure 9: 1D pressure distribution from the wellbore to the domain boundary along $Y = 300$ m after (a) 0.5 day and (b) 1 day of shallow water flow for permeability sensitivity.

4.2. Permeability. Permeability describes the ability of water to flow in the porous layer. In a heterogeneous subsurface environment, permeability values can vary in a certain range. Three permeability values are tested: 0.5 D, 1.0 D (base case), and 1.5 D. Other parameters are the same as the base case.

Similar to the previous plots, Figure 9 shows the pressure distribution from the wellbore to the boundary of the domain along $Y = 300$ m. Figure 10 shows the distribution of stress.

Figure 9 shows that a greater permeability value results in a lower pressure distribution profile. The reason is that when permeability is large, it becomes easy for the water to flow from the porous media to the wellbore. Therefore, the corresponding pressure drainage is significant. A permeability of 0.5 D leads to the highest pressure profile, as it indicates the slowest flow drainage. In addition, as time increases, pressures uniformly decrease. This is caused by the drainage at the wellbore. Figure 10 presents the spatial distribution of stress along the observation line. Although discrepancies between stress curves are relatively small, trends show that permeability values are negatively correlated with stress values. For a low permeability (0.5 D in this case), the fluid drainage is relatively insignificant, leading to small

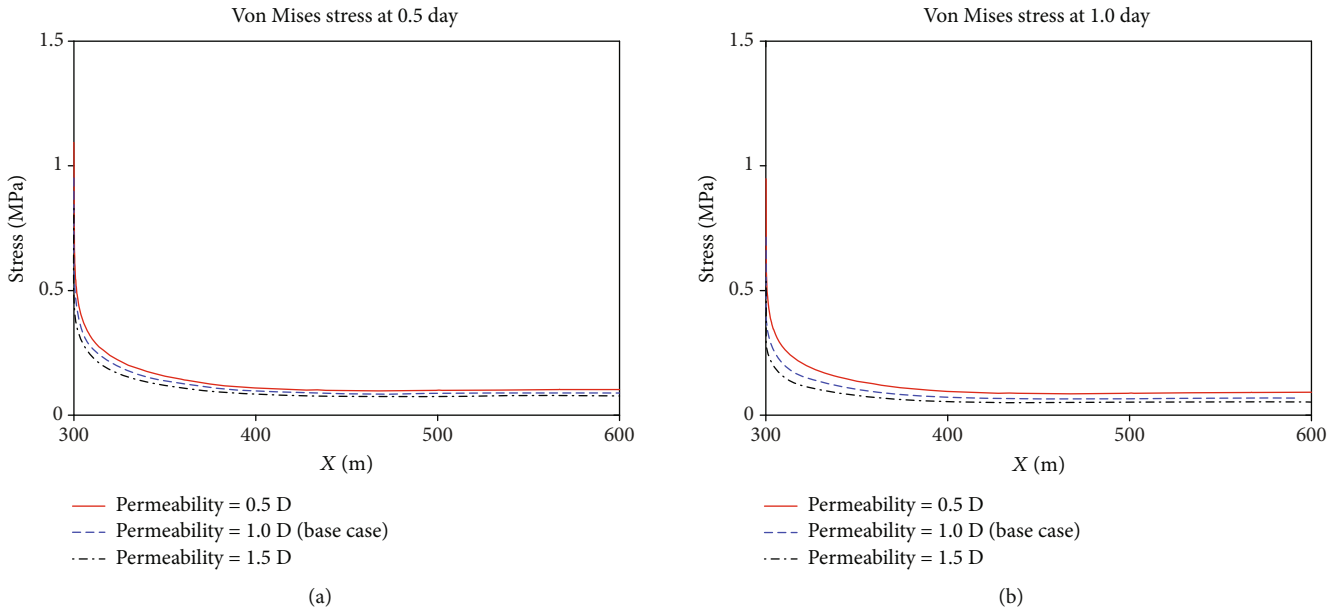

Figure 10: 1D stress distribution from the wellbore to the domain boundary along $Y = 300$ m after (a) 0.5 day and (b) 1 day of shallow water flow for permeability sensitivity.

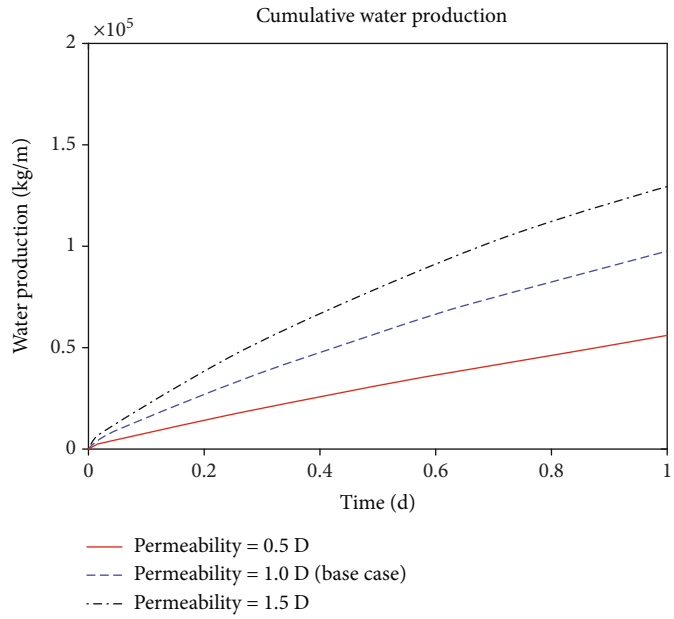

Figure 11: Cumulative water production at the wellbore during one day of shallow water flow for permeability sensitivity.

deformation and stress magnitudes. Since drainage is not strong near the boundary, stress magnitudes decrease as it moves from the wellbore to the domain boundary. Besides, stress magnitudes decrease with time. This can also be explained by the fact that the pressure differences between the wellbore and the porous media decrease with time, and this decrease leads to less pore volume deformation.

Figure 11 shows the cumulative water production in the wellbore caused by shallow water flow. Since a large permeability represents a good capability of water flow in porous media, a permeability of 1.5 D corresponds to the highest water production in this case. The lowest permeability of 0.5 D results in the smallest cumulative water production, which is more preferable in deepwater drilling.

4.3. Porosity. Porosity is the ratio of the pore volume to the bulk volume in porous media. Porosity values in deepwater shallow sediments are usually large [19]. Porosity is a critical property for fluid flow in porous media. While the other parameters are kept the same, three porosity values of 0.3, 0.4 (base case), and 0.5 are used in the simulated.

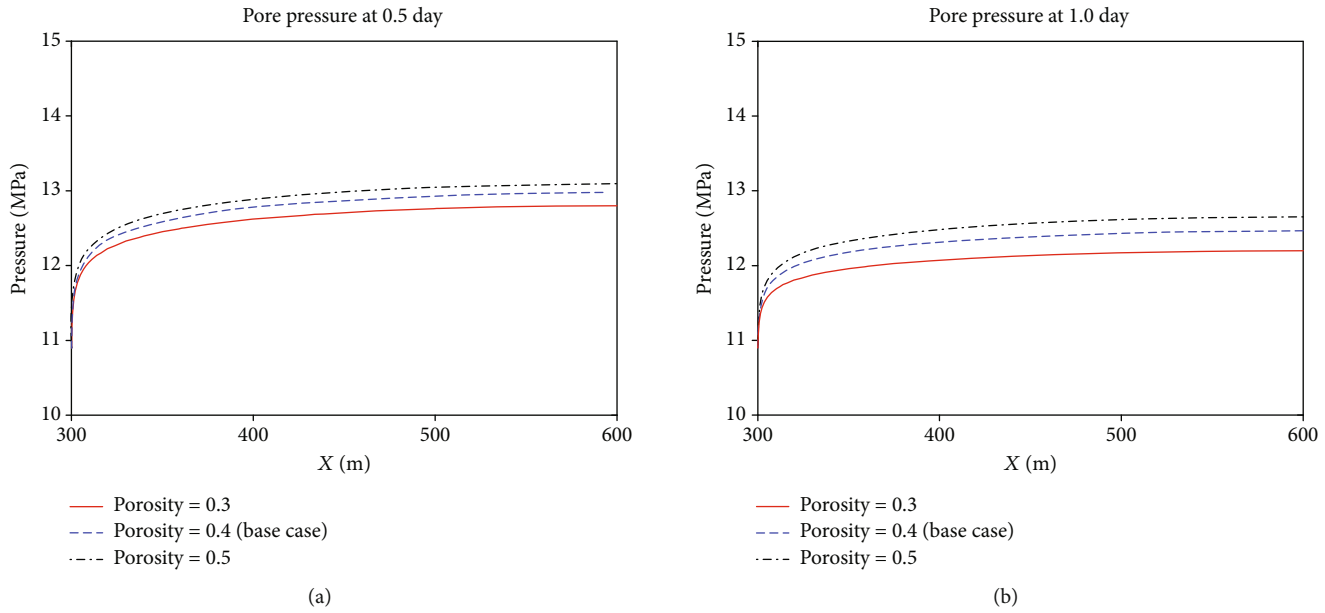

FIGURE 12: 1D pressure distribution from the wellbore to the domain boundary along $Y = 300$ m after (a) 0.5 day and (b) 1 day of shallow water flow for porosity sensitivity.

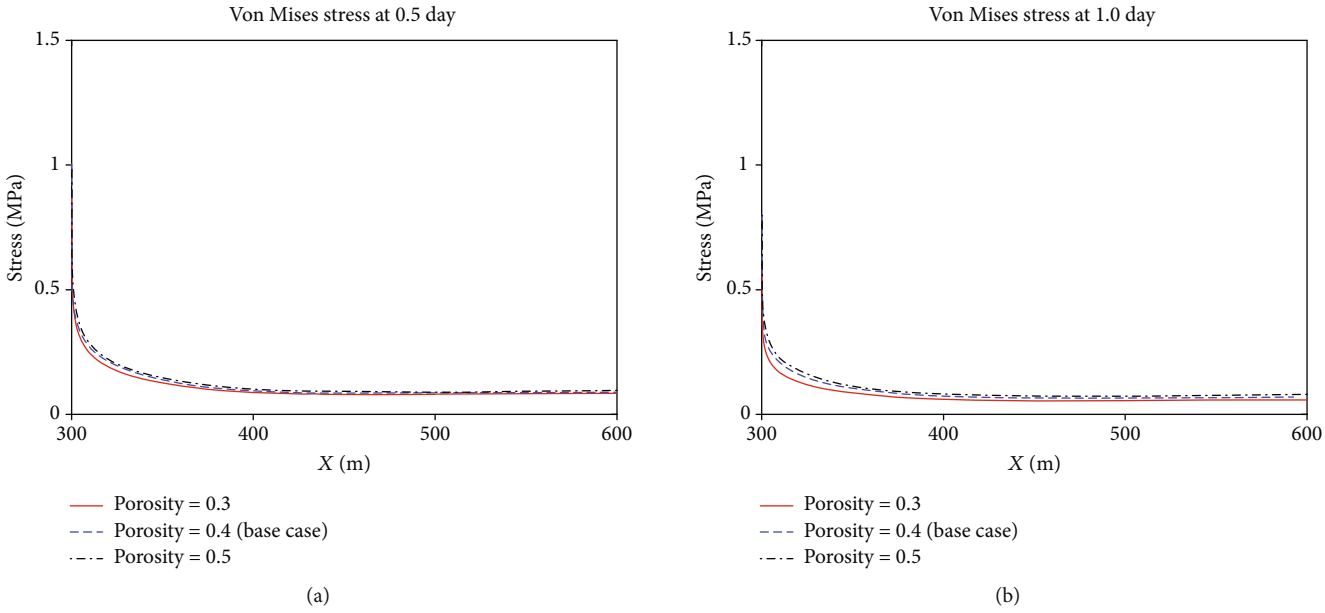

FIGURE 13: 1D stress distribution from the wellbore to the domain boundary along $Y = 300$ m after (a) 0.5 day and (b) 1 day of shallow water flow for porosity sensitivity.

Using the same 1D observation line as previously, Figures 12 and 13, respectively, present the comparisons of pressure and stress profiles from the wellbore to the boundary for three porosity cases at two separate time steps.

Figure 12 indicates that porosity values are negatively correlated with pressure profile heights. This is because a higher porosity represents a higher fluid storage capacity of the porous media, while a smaller porosity indicates lower fluid storage and more fluid drainage. The effects of time of pressure are significant as fluid drainage becomes more significant with time. Figure 13 shows that the differences between stress results are relatively small. As a high porosity leads to a high-pressure profile and a greater pressure difference between the porous media and the wellbore, the porous media experience faster pressure change and more pore volume change. Therefore, a greater porosity value corresponds to a higher stress profile.

Figure 14 presents the effects of porosity on cumulative water production in the wellbore. Results indicate that a greater porosity corresponds to a lower cumulative water production. This is because a greater porosity implies a lower water storage capability in the porous media.

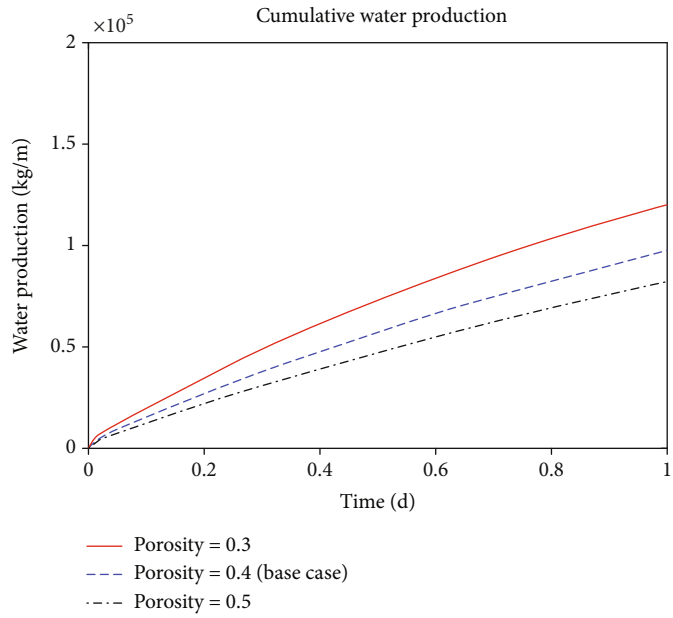

Figure 14: Cumulative water production at the wellbore during one day of shallow water flow for porosity sensitivity.

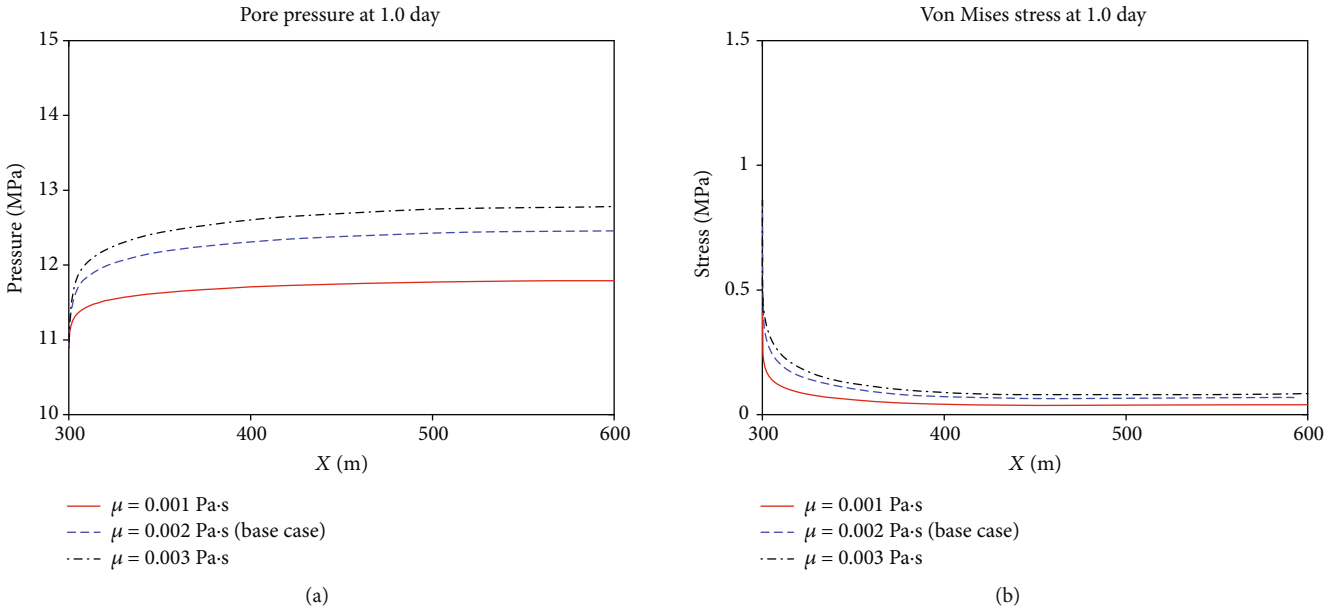

Figure 15: 1D (a) pressure and (b) stress distributions from the wellbore to the domain boundary along $Y = 300$ m after 1 day of shallow water flow for viscosity sensitivity.

4.4. Water Viscosity. Viscosity is a fluid property for water encountered in deepwater drilling. It represents the friction between fluid molecules. In this section, the effects of three water viscosity values on pressure, stress, and water production are investigated.

Figure 15 presents the 1D pressure and stress distributions along the observation line after one day of shallow water flow. Figure 15(a) indicates that water viscosity is positively correlated with pressure in the sediments. Large water viscosity implies slow water flow and fluid drainage, which result in high pore pressure. Large viscosity also leads to a high-stress profile in Figure 15(b), as large viscosity implies greater pressure differences between the wellbore and porous media and more spatial pore volume change.

Figure 16 shows the water production in the wellbore for three viscosity cases. Since low viscosity fluid is easy to flow in the porous media, the lowest viscosity leads to the largest cumulative water production.

4.5. Young's Modulus. Young's modulus represents the stiffness of the solid sediments. Although bulk modulus directly represents the stiffness of the subsurface solid, Young's modulus is investigated here due to the facts that it is very hard to directly measure bulk modulus and that bulk modulus and

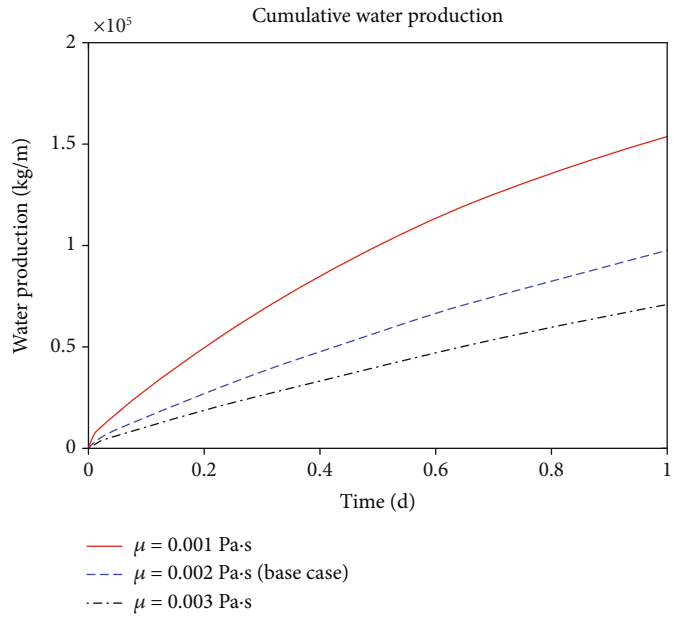

Figure 16: Cumulative water production at the wellbore during one day of shallow water flow for viscosity sensitivity.

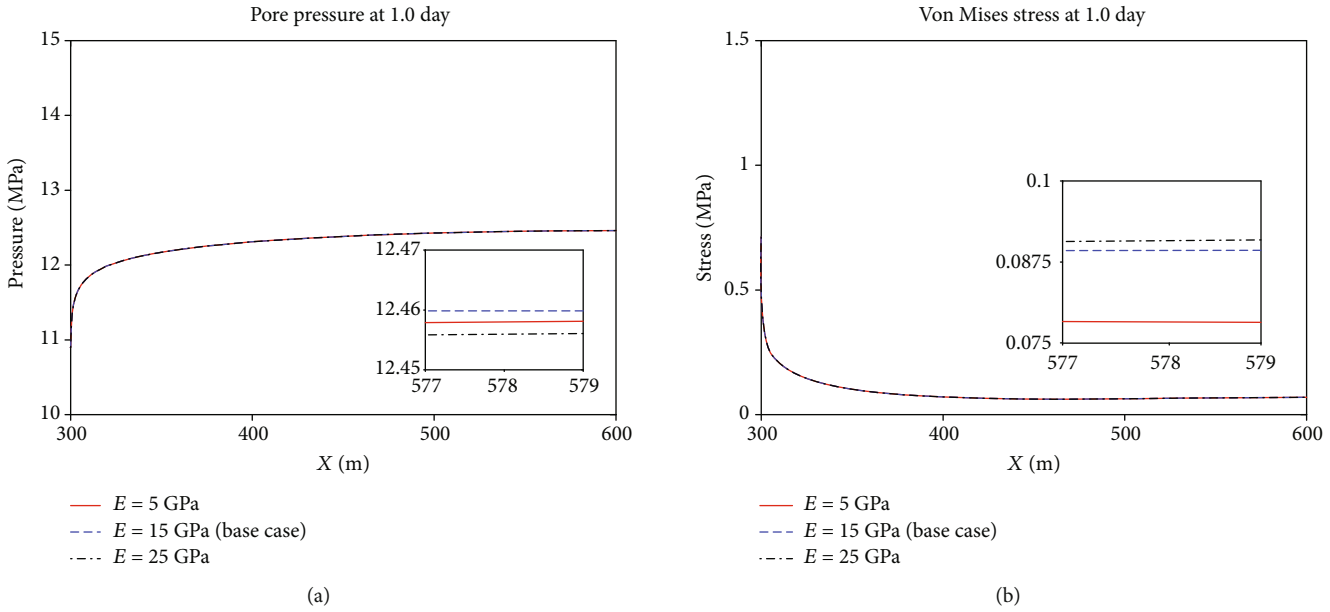

Figure 17: 1D (a) pressure and (b) stress distributions from the wellbore to the domain boundary along $Y = 300$ m after 1 day of shallow water flow for Young's modulus sensitivity.

Young's modulus have a linear correlation via Poisson's ratio based on linear elasticity assumption [35]. Three Young's modulus values are studied: 5 GPa, 15 GPa (base case), and 25 GPa.

Figure 17 presents 1D pressure and stress distributions along the observation line after one day of shallow water flow. Results show that Young's modulus has limited effects on pressure and stress. The smallest Young's modulus corresponds to the lowest pressure and stress profiles. This is because a low Young's modulus implies a low material stiffness which yields a weak water storage capability and more pressure drainage. Figure 18 shows the comparison for cumulative water productions in the wellbore. Since Young's modulus of 5 GPa leads to the greatest fluid drainage, it also leads to the highest water production.

4.6. Water Compressibility. Water compressibility depicts the change in water volume under the effect of pressure. It is an important fluid property for the study of shallow water flow in the porous media. In this sensitivity analysis, three water compressibility values are simulated: 3×10^{-10} 1/Pa, 4.5×10^{-10} 1/Pa (base case), and 6×10^{-10} 1/Pa.

Figure 19 records the pressure and stress distributions along the observation line after one day of shallow water flow

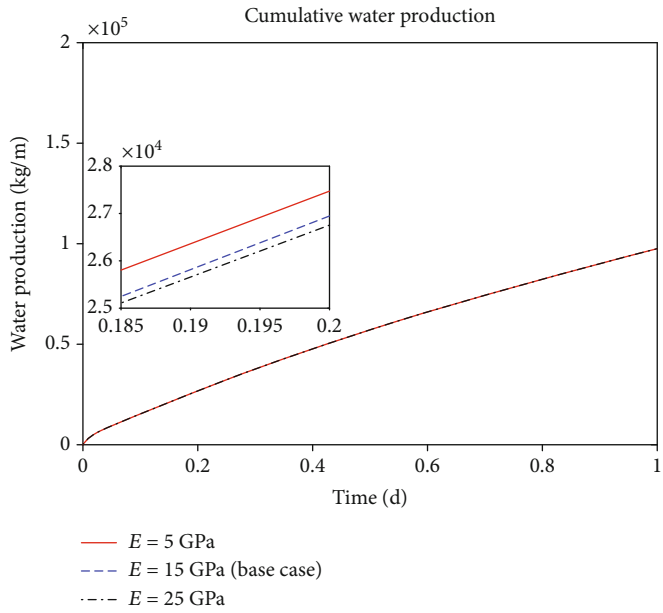

FIGURE 18: Cumulative water production at the wellbore during one day of shallow water flow for Young's modulus sensitivity.

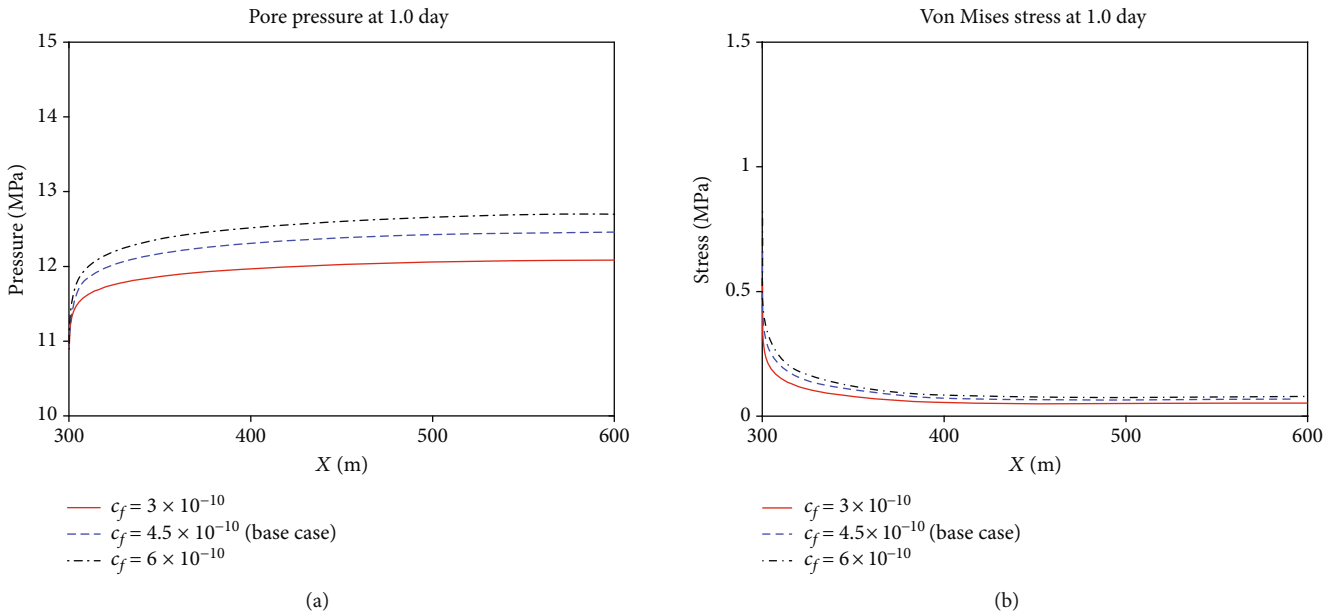

FIGURE 19: 1D (a) pressure and (b) stress distributions from the wellbore to the domain boundary along $Y = 300$ m after 1 day of shallow water flow for water compressibility sensitivity.

for water compressibility sensitivity. For the case with water compressibility of 3×10^{-10} 1/Pa, water is less compressible, indicating less storage in the pore volume. As a result, more fluid is produced to the wellbore and greater pressure drainage is generated. Since more spatial pore volume change is obtained by a lower water compressibility, a lower spatial stress profile is obtained.

Figure 20 presents the comparison between water productions in the wellbore for three different water compressibility values. Water compressibility of 3×10^{-10} 1/Pa leads to the highest cumulative production since this compressibility yields the most significant fluid drainage. It is noted that the effect of water compressibility on cumulative productions is not very noticeable for the early stages of shallow water flow and the effect becomes significant when it gets close to one day. This is different from the observations in other sensitivity analyses in Figures 8, 11, 14, and 16 where the investigated parameters take effects on cumulative productions from the beginning of shallow water flow.

4.7. Quantitative Understanding of Effects of Investigated Parameters. Relative impacts of the investigated parameters in the parametric study are quantified in this section. In each sensitivity analysis, $\Delta\omega$, the change of the investigated

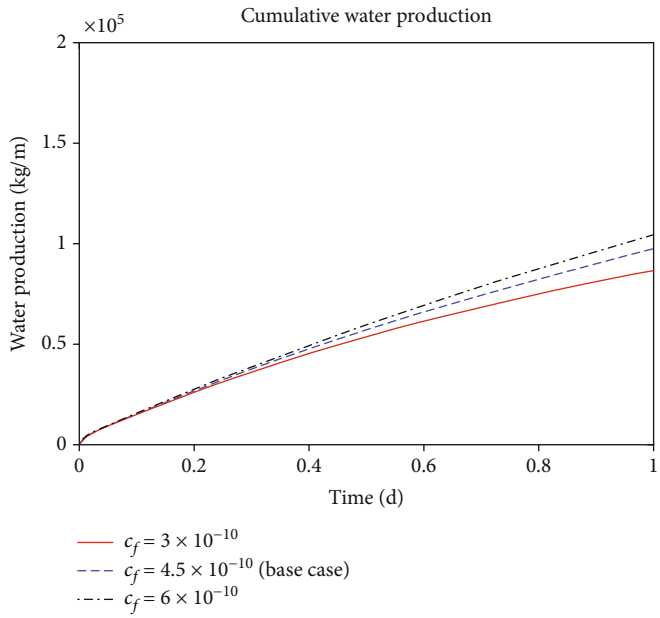

Figure 20: Cumulative water production at the wellbore during one day of shallow water flow for water compressibility sensitivity.

Table 4: Relative impacts $\Delta\theta/\Delta\omega$ of six sensitivity analysis parameters on pressure and stress at three time steps.

Time (d)	Overpressure		Permeability		Porosity	
	Pressure	Stress	Pressure	Stress	Pressure	Stress
0.1	18.47%	99.98%	1.62%	0.58%	1.24%	3.69%
0.5	15.13%	99.94%	4.37%	35.77%	3.80%	33.70%
1.0	11.80%	99.92%	6.84%	64.59%	5.88%	64.47%
Time (d)	Water viscosity		Young's modulus		Water compressibility	
	Pressure	Stress	Pressure	Stress	Pressure	Stress
0.1	1.89%	4.36%	0.10%	2.24%	1.72%	5.44%
0.5	5.30%	45.69%	0.03%	0.48%	5.25%	45.96%
1.0	7.69%	79.05%	0.01%	0.10%	8.00%	85.48%

parameter in percentage, is obtained. Then, $\Delta\theta$, the corresponding changes in the primary variables in percentage (i.e., pressure, stress, and cumulative water production in this study), are obtained. Thus, the relative impacts of the currently investigated parameter on pressure, stress, and cumulative water production in the wellbore can be quantified as the ratio of $\Delta\theta/\Delta\omega$.

Table 4 records the relative impacts of totally six investigated parameters on pressure and stress. Note that pressure and stress values used here are the averaged values along the 1D spatial observation line aforementioned. Results are reported for three time steps of 0.1 day, 0.5 day, and 1.0 day. Results indicate that as time evolves, impacts of overpressure and Young's modulus on pressure and stress exhibit declining trends, while the impacts of the other four parameters exhibit increasing trends. In general, parametric effects on pressure are smaller than those effects on stress. In summary, based on results at the time step of one day, the effects of investigated parameters on pressure and stress can be ranked from the greatest to the smallest as overpressure > water compressibility > water viscosity > permeability > porosity > Young's modulus.

Table 5: Relative impacts $\Delta\theta/\Delta\omega$ of six sensitivity analysis parameters on cumulative water production in the wellbore during one day of shallow water flow.

Overpressure	Permeability	Porosity
99.91%	85.10%	78.58%
Water viscosity	Young's modulus	Water compressibility
80.65%	0.79%	33.94%

Similarly, the relative impacts of investigated parameters on cumulative water production in the wellbore during one day of shallow water flow are documented in Table 5. Based on the result, the effects of investigated parameters on cumulative water production can be ranked from the greatest to the smallest as overpressure > permeability > water viscosity > porosity >water compressibility > Young's modulus.

The two ranks indicate that overpressure is the most influential parameter affecting in-situ pressure and stress evolutions and water production when shallow water flow is encountered, while Young's modulus has the smallest effect. However, the rank of influences of the other four parameters is not uniform in the context of pressure, stress, and water production.

5. Conclusion and Recommendation

In this work, a finite element model that couples deformation of sediments and fluid flow in porous media is established to investigate the characteristics of pressure and stress in the near-well area when shallow water flow is encountered. The induced water production in the wellbore is also quantified. As a contribution, this work focuses on the coupled

hydraulic-mechanical processes in the near-well shallow-water-flow area and presents a systematic parametric study. The results in this study also contribute to the understanding of near-well pressure/stress evolutions and serve as a reference for the remediation of well control problems caused by shallow water flow during deepwater drilling.

In conclusion:

(1) Overpressure is the most influential parameter that affects the temporal and spatial evolutions of pressure and stress in the near-well area. It also has the most significant effect on shallow-water-flow-induced water production in the wellbore during deepwater drilling

(2) Young's modulus has the most limited impact on near-well pressure, stress, and water production in the wellbore

(3) Small overpressure, low permeability, large porosity, high water viscosity, and small water compressibility all contribute to low water production in the wellbore

(4) In the near-well area, locations closer to the wellbore experience greater stress magnitudes. This is caused by the fact that water flow velocity and pressure decrease are more significant at areas closer to the wellbore

Based on the simulation results in this study, it is noted that, in terms of depletion-induced hydromechanical behaviors, overpressure is the most important parameter to control during drilling through deepwater shallow sediments while the mechanical property represented by the modulus of the sediments has a rather limited effect. However, the significance of the mechanical properties of sediments should not be neglected as it affects how sediments enter the plastic region.

Data Availability

(1) The Terzaghi's problem validation data used to support the findings of this study for Section 2.5 "Model Validation" have been deposited in the OnePetro repository (10.2118/182665-MS). (2) The numerical model input data used to support the findings of this study for Section 3.2 "Input parameters" have been deposited in the OnePetro repository (10.2118/67772-MS). (3) The numerical model input data used to support the findings of this study for Section 3.2 "Input parameters" have been deposited in ScienceDirect (10.1016/j.marpetgeo.2009.01.018).

Conflicts of Interest

The authors declare that they have no conflicts of interest.

Acknowledgments

This work was financially supported by the National Natural Science Foundation of China (Grant No. 51904314), by the Fundamental Research Funds for the Central Universities and the Science Foundation of China University of Petroleum, Beijing (Grant No. 2462018YJRC031), and by the Independent Research Project of the State Key Laboratory of Petroleum Resources and Prospecting, China University of Petroleum, Beijing (Grant No. PRP/indep-4-1813), and by the Research Foundation of China University of Petroleum-Beijing at Karamay (Grant No. XQZX20200009).

References

[1] W. Furlow, "Shallow water flows: how they develop; what to do about them," *Offshore Magazine*, vol. 58, no. 9, p. 70, 1998.

[2] R. M. Ostermeier, J. H. Pelletier, C. D. Winker, J. W. Nicholson, F. H. Rambow, and K. M. Cowan, "Dealing with shallow-water flow in the Deepwater Gulf of Mexico," *The Leading Edge*, vol. 21, no. 7, pp. 660–668, 2002.

[3] S. G. Wu, Y. B. Sun, X. J. Wang, Q. Zhao, F. Liu, and D. D. Dong, "Geophysical signature and detection of shallow water flow in the Deepwater basin of the northern South China Sea," *Diqiu Wuli Xuebao*, vol. 53, no. 7, pp. 1681–1690, 2010.

[4] S. McGiveron and J. Jong, "A case study and model of shallow water flow (SWF) from Sabah deepwater drilling operations, offshore Malaysia," *Warta Geologi*, vol. 44, no. 2, pp. 39–47, 2018.

[5] X. Zhang, Y. Sun, S. Wu, and D. Dong, "Geophysical signature of the shallow water flow in the Deepwater Basin of the northern South China Sea," *Journal of Ocean University of China*, vol. 17, no. 4, pp. 791–798, 2018.

[6] Y. Shen, T. Tang, R. Zuo, Z. Zhang, and Y. Wang, "Identification of shallow water flow using multicomponent seismic and GPR attributes in the deepwater basin of the northern South China Sea," *Indian Journal of Geo Marine Sciences*, vol. 47, no. 9, 2018.

[7] L. Eoff and J. Griffith, "Acrylate monomer solution stops artesian water, geopressured sand flows," *Oil & Gas Journal*, vol. 96, no. 44, pp. 89–91, 1998.

[8] D. R. McConnell, "Optimizing deepwater well locations to reduce the risk of shallow-water-flow using high-resolution 2D and 3D seismic data," in *Offshore Technology Conference*, Houston, TX, USA, May 2000.

[9] S. Mallick and N. C. Dutta, "Shallow water flow prediction using prestack waveform inversion of conventional 3D seismic data and rock modeling," *The Leading Edge*, vol. 21, no. 7, pp. 675–680, 2002.

[10] S. Lu, "Seismic characteristics of two deep-water drilling hazards: shallow-water flow sands and gas hydrate," PhD Thesis, The University of Texas at Dallas, 2003.

[11] S. Lu, G. A. McMechan, and A. Liaw, "Identification of shallow-water-flow sands by Vp/Vs inversion of conventional 3D seismic data," *Geophysics*, vol. 70, no. 5, pp. O29–O37, 2005.

[12] D. R. McConnell, Z. Zhang, and R. Boswell, "Review of progress in evaluating gas hydrate drilling hazards," *Marine and Petroleum Geology*, vol. 34, no. 1, pp. 209–223, 2012.

[13] B. Zhang, J. Yang, T. Sun et al., "Prediction model of shallow geological hazards in deepwater drilling based on a hybrid computational approach," in *52nd US Rock Mechanics/Geomechanics Symposium*, Seattle, WA, USA, June 2018.

[14] L. F. Eaton, "Drilling through deepwater shallow water flow zone at URSA," in *SPE/IADC Drilling Conference*, Amsterdam, Holland, March 1999.

[15] P. C. Schuberth and M. W. Walker, "Shallow water flow planning and operations: Titan#1 exploration well, deepwater Gulf of Mexico," in *SPE/IADC drilling conference*, Amsterdam, Netherlands, March 1999.

[16] C. D. Winker and R. J. Hannaford, "Geology of shallow-water flow at Ursa: 2. Drilling principles and practice," in *Offshore Technology Conference*, Houston, TX, USA, April-May 2007.

[17] C. D. Winker and R. J. Stancliffe, "Geology of shallow-water flow at Ursa: 1. Settings and causes," in *Offshore Technology Conference*, Houston, TX, USA, April-May 2007.

[18] A. Blischke, Þ. S. Arnarson, and B. Richter, "Offshore geohazards to keep in mind during prospecting and exploration activities of the Jan Mayen Micro-Continent area," *30th Nordic Geological Winter Meeting*, 2012, Reykjavik, Iceland, January 2012, 2012.

[19] R. M. Ostermeier, J. H. Pelletier, C. D. Winker, and J. W. Nicholson, "Trends in shallow sediment pore pressures-Deepwater Gulf of Mexico," in *SPE/IADC drilling conference*, Amsterdam, Netherlands, February-March 2001.

[20] A. R. Huffman and J. P. Castagna, "The petrophysical basis for shallow-water flow prediction using multicomponent seismic data," *The Leading Edge*, vol. 20, no. 9, pp. 1030–1052, 2001.

[21] N. T. T. Binh, T. Tokunaga, T. Nakamura et al., "Physical properties of the shallow sediments in late Pleistocene formations, Ursa Basin, Gulf of Mexico, and their implications for generation and preservation of shallow overpressures," *Marine and Petroleum Geology*, vol. 26, no. 4, pp. 474–486, 2009.

[22] J. S. Reece, P. B. Flemings, B. Dugan, H. Long, and J. T. Germaine, "Permeability-porosity relationships of shallow mudstones in the Ursa Basin, northern Deepwater Gulf of Mexico," *Journal of Geophysical Research: Solid Earth*, vol. 117, no. B12, 2012.

[23] Z. Gong, S. Ren, L. Zhang, P. Zhang, Y. Xu, and L. Yu, "Numerical simulation of water and sand blowout when drilling through shallow water flow sediments during deepwater drilling," *Offshore Technology Conference*, 2017, Houston, TX, USA, May 2017, 2017.

[24] S. Ren, Y. Liu, Z. Gong et al., "Numerical simulation of water and sand blowouts when penetrating through shallow water flow formations in deep water drilling," *Journal of Ocean University of China*, vol. 17, no. 1, pp. 17–24, 2018.

[25] J. Sun, S. Wu, J. Deng et al., "Numerical simulation of mechanical compaction of deepwater shallow sediments," *Journal of Ocean University of China*, vol. 17, no. 1, pp. 53–64, 2018.

[26] K. Terzaghi, "Die Berechnung der Durchassigkeitsziffer des Tones aus dem Verlauf der hydrodynamischen Spannungserscheinungen," *Akademie der Wissenschaften in Wien. Sitzungsberichte*, vol. 11, pp. 105–124, 1923.

[27] K. Terzaghi, *Erdbaumechanik Auf Bodenphysikalischer Grundlage (Mechanics of Earthworks Based on Rudiments of Soil Physics)*, Deuticke, 1925.

[28] M. A. Biot, "General theory of three-dimensional consolidation," *Journal of Applied Physics*, vol. 12, no. 2, pp. 155–164, 1941.

[29] M. A. Biot, "Theory of elasticity and consolidation for a porous anisotropic solid," *Journal of Applied Physics*, vol. 26, no. 2, pp. 182–185, 1955.

[30] N. P. Roussel, H. Florez, and A. A. Rodriguez, "Hydraulic fracture propagation from infill horizontal wells," in *SPE Annual Technical Conference and Exhibition*, New Orleans, Louisiana, USA, September-October 2013.

[31] F. O. Alpak, "Robust fully-implicit coupled multiphase-flow and geomechanics simulation," *SPE Journal*, vol. 20, no. 6, pp. 1–366, 2015.

[32] X. Guo, K. Wu, C. An, J. Tang, and J. Killough, "Numerical investigation of effects of subsequent parent well injection on interwell fracturing interference using reservoir-geomechanics-fracturing modeling," *SPE Journal*, vol. 24, no. 4, pp. 1884–1902, 2019.

[33] F. Zhang, M. An, B. Yan, Y. Wang, and Y. Han, "A novel hydro-mechanical coupled analysis for the fractured vuggy carbonate reservoirs," *Computers and Geotechnics*, vol. 106, pp. 68–82, 2019.

[34] D. Yang, G. J. Moridis, and T. A. Blasingame, "A fully coupled multiphase flow and geomechanics solver for highly heterogeneous porous media," *Journal of Computational and Applied Mathematics*, vol. 270, pp. 417–432, 2014.

[35] X. Guo, K. Wu, and J. Killough, "Investigation of production-induced stress changes for infill well stimulation in Eagle Ford Shale," *SPE Journal*, vol. 23, no. 4, pp. 1372–1388, 2018.

[36] T. J. R. Hughes, *The Finite Element Method: Linear Static and Dynamic Finite Element Analysis*, Prentice-Hall, Englewood Cliffs, 1987.

[37] D. P. C. Mazzei, *Normalized Mechanical Properties of Resedimented Gulf of Mexico Clay from Integrated Ocean Drilling Program Expedition Leg 308*, MS Thesis, Northeastern University, United States, 2007.

[38] C. H. Cong, L. O. Jianjun, and L. I. Ganxian, "Experimental study on mechanical properties of seafloor sediments of deep South China Sea," *The Ocean Engineering*, vol. 33, no. 4, pp. 108–114, 2015.

[39] J. Kim, H. A. Tchelepi, and R. Juanes, "Stability, accuracy, and efficiency of sequential methods for coupled flow and geomechanics," *SPE Journal.*, vol. 16, no. 2, pp. 249–262, 2013.

[40] R. H. Dean, X. Gai, C. M. Stone, and S. E. Minkoff, "A comparison of techniques for coupling porous flow and geomechanics," *SPE Journal*, vol. 11, no. 1, pp. 132–140, 2013.

[41] J. Geertsma, "The effect of fluid pressure decline on volumetric changes of porous rocks," *Transactions of the AIME*, vol. 210, no. 1, pp. 331–340, 1957.

[42] M. A. Biot and D. G. Willis, "The elastic coefficients of the theory of consolidation," *Journal of Applied Mechanics*, vol. 24, pp. 594–601, 1957.

[43] A. Verruijt, *Computational Geomechanics*, Kluwer Academic Publishers, London, 1995.

[44] X. Guo, J. Kim, and J. Killough, "Hybrid MPI-OpenMP scalable parallelization for coupled non-isothermal fluid-heat flow and elastoplastic geomechanics," *SPE Reservoir Simulation Conference*, 2017, Montgomery, TX, USA, February 2017, 2017.